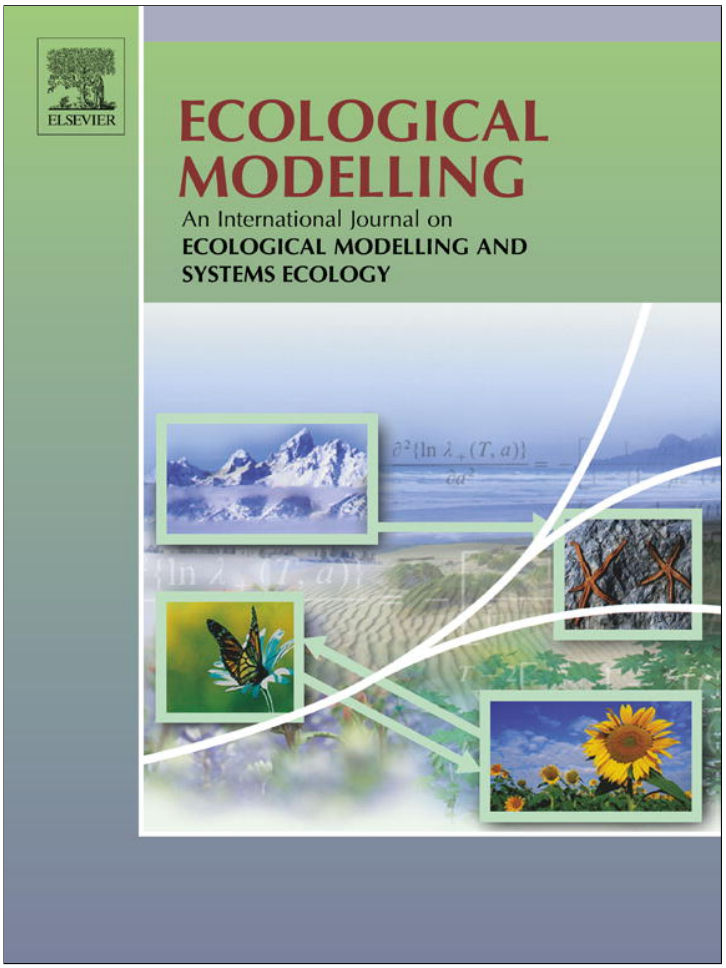

Ecological Modelling 257 (2013) 25–35

Contents lists available at SciVerse ScienceDirect

Ecological Modelling

journal homepage: www.elsevier.com/locate/ecolmodel

SAILHFlood: A radiative transfer model for flooded vegetation

M.E. Beget[a,*], V.A. Bettachini[a,1], C.M. Di Bella[a,b], F. Baret[c]

[a] Instituto Nacional de Tecnología Agropecuaria, Buenos Aires, Argentina
[b] Consejo de Investigaciones Científicas y Técnicas, Buenos Aires, Argentina
[c] INRA, Unite Environnement Mediterranéen et Modélisation des Agro-Hydrosystèmes, UMR1114, Site Agroparc, 84914 Avignon Cedex 09, France

ARTICLE INFO

Article history:
Received 24 July 2012
Received in revised form 15 February 2013
Accepted 18 February 2013

Keywords:
Reflectance model
Surface water
SAILH
Wetlands

ABSTRACT

In this manuscript we present a radiative transfer model for submerged vegetation called *SAILHFlood*. It simulates reflectance for a partial submerged canopy from vegetation variables, water level, measurement geometry and soil reflectance. It is a version of the proven *SAILH* model in which, two vegetation layers are included instead of one: the emerged vegetation layer and the submerged vegetation layer, for which the water attenuation is considered. The model validation was performed with a experiment in laboratory conditions varying leaf area index, water level and illumination and observation angles. A least square linear fit of simulated data used to reproduce measured data shows a satisfactory root mean square error (*RMSE*) of 0.0355, and a spectral angle of 0.2591 radians. The model could be applied to the diversity of vegetation found in flooded situations, both to understand spectral behavior of these environments under different scenarios and to estimate vegetation variables from model inversion.

1. Introduction

The inversion of radiative transfer models is one of the available methodologies for plant variables estimation. However, particular situations, as flooded environments, require special attention using remote sensing as water modifies the spectral response of vegetation covers. Canopy reflectance is influenced by leaves optical properties and by their structure. Shape, size and distribution of leaves in the canopy, leaf area index (LAI) and the soil cover proportion determine the radiation reflected, transmitted and absorbed by vegetation tissues (*e.g.* Guyot et al., 1992; Jacquemoud et al., 1996). In flooded canopies the surrounding water absorbs radiation in the mid-infrared portion of the electromagnetic spectrum and consequently, reflectance in this portion is close to zero. In contrast, reflectance in visible and near infrared bands usually presents high variability (*e.g.* Jerlov, 1968; Bilge et al., 2003; Han and Rundquist, 2003; Beget and Di Bella, 2007). This variability depends on the reflectance of the submerged soil, water depth and the amount of the suspended particles and their optical properties (*e.g.* Baret, 1990). The abundance of optically active components, such as phytoplankton, suspended minerals and dissolved organic carbon affects water turbidity directly (Bilge et al., 2003). The water that is most turbid of all has higher reflectance levels in the longest wavelengths of the visible spectrum.

In situations where the vegetation is submerged, the spectral response of vegetation–water system has a variable pattern depending on the interaction between both components (*e.g.* Beget and Di Bella, 2007). For example, spectral signature depends not only on water level but also on the canopy architecture, leaf area and its distribution over the water column. Water attenuates the radiation reaching submerged plant tissues such as reflected or transmitted by canopy. This attenuation is more important in the infrared wavelengths and even more in the short-wave infrared band (Jerlov, 1968).

Most research on the spectral behavior of flooded vegetation environments have been conducted through the study of different vegetation covers (*e.g.* Moreau and Le Toan, 2003; Oguro et al., 2003; Xiao et al., 2005). Other authors have conducted experimental studies using remote sensors with a high spatial and spectral resolution in order to characterize the reflectance of canopies under controlled conditions of waterlogging (*e.g.* Han and Rundquist, 2003; Beget and Di Bella, 2007). These studies showed, in general: the spectral behavior of flooded vegetation depends mainly on canopy structure (*LAI*); the proportion of ground covered by vegetation; the water depth, and the relation and amount of emerged and submerged leaf area. Those studies made possible, in the case of rice, to assess crop stage (flood and transplantation) and to estimate

* Corresponding author at: Los Reseros y Las Cabañas s/n, 1686 Hurlingham, Buenos Aires, Argentina. Tel.: +54 11 4621 1684; fax: +54 11 4621 5663.
E-mail addresses: mbeget@cnia.inta.gov.ar (M.E. Beget), vbettach@itba.edu.ar (V.A. Bettachini), cdibella@inta.gov.ar (C.M. Di Bella), baret@avignon.inra.fr (F. Baret).
[1] Present address: Laboratorio de Optoelectrónica, Instituto Tecnológico de Buenos Aires, Av. Eduardo Madero 399, C1106ACD Buenos Aires, Argentina.

0304-3800/$ – see front matter © 2013 Elsevier B.V. All rights reserved.
http://dx.doi.org/10.1016/j.ecolmodel.2013.02.025

the sown area (Xiao et al., 2005). In the case of forage resources, estimations of forage availability were performed through the assessment of biomass variation during the rainy period in which the plants covered the greatest fraction of soil (*e.g.* Moreau and Le Toan, 2003 for the Bolivian Altiplano).

Despite such progress, several questions remain unanswered regarding the factors that determine the spectral response of water and vegetation interacting with each other. For example, although it is known that the spectral response of a flooded canopy varies with water depth (Han and Rundquist, 2003; Beget and Di Bella, 2007), it is not known which is the contribution of submerged plants tissues to total reflectance. As the vegetation has bidirectional behavior, meaning that the reflectance depends on illumination and observation angles (Kuusk, 1985; Schaepman-Strub et al., 2006), the special situation of flooded vegetation was not analyzed yet.

Radiative transfer modeling techniques have been developed and improved during the last three decades, yielding a contribution to the understanding of biophysical processes that determine canopy reflectance. Currently there are several models available able to simulate the spectral response of vegetation (see RAMI exercise, Pinty et al., 2001, 2004; Widlowski et al., 2007). In our work the *SAILH* model was chosen because it provides an appropriate balance between precision and simplicity (Andrieu et al., 1997; Weiss et al., 2000). This balance makes the model a common choice in the research community, as well as for application of model in direct and inverse mode, as for model improvement and additions (Jacquemoud et al., 2009). Thus although other models represent more accurately fluxes, a first approach was proposed toward the problematic presented by submerged vegetation to use the relatively simple *SAILH*. This simplicity is based in assuming that radiation fluxes (upward and downward) are isotropic. This oversimplification clearly undermines the quantitative accuracy of the predictions. Nevertheless this allows following closely the SAILH proposal of two diffuse and two direct fluxes in each layer. The original specification of the model was kept in order to perform, in future, quantitative evaluations of assumptions.

In the system considered by *SAILH* model, the air is the propagation medium; however, in partially flooded vegetation, part of the propagation medium becomes water. Because water scatters and absorbs radiation, reflectance models have the limitations already mentioned when simulating canopy reflectance of partially or completely flooded vegetation.

Although the *SAILH* model was improved to cover several aspects of vegetation, it still has to include the presence of surface water. Considering the importance of flooded areas, such as natural grasslands, wetlands and rice crops in the provision of ecosystem goods and services, there is a clear interest in extending the model to cover these systems. It was the aim of our work to develop a radiative transfer model for partially submerged vegetation based on the *SAILH* that we named *SAILHFlood*. The present work focuses in validating the core assumptions of the *SAILH* model working on submerged vegetation not on real situations but on the idealized one experimented in laboratory conditions.

1.1. The SAILH model

The *SAILH* model, developed by Verhoef (1984, 1985), is in its turn based on the Suits model (Suits 1972). The Suits model proposes the existence of two downward and two upward radiation fluxes that are affected by scattering and extinction at the plant canopy that is assumed as a turbid medium. Relations between fluxes are expressed as a linear differential equation system with nine coefficients, named the *Duntley* equations, which are described by the radiative transfer in the canopy:

$$\begin{aligned}\frac{dE_s}{dx} &= kE_s\\ \frac{dE_-}{dx} &= -sE_s + aE_- - \sigma E_+\\ \frac{dE_+}{dx} &= -s'E_s + \sigma E_- - aE_+\\ \frac{dE_o}{dx} &= wE_s + vE_- + uE_+ - KE_o\end{aligned} \tag{1}$$

In the *Duntley* equations x represents the vertical dimension with upward orientation; E_s direct solar irradiance; E_- and E_+ diffuse downward and upward irradiance, respectively; E_o is π times the radiance in the observer direction; k and K extinction coefficients for E_s and E_o, respectively; a attenuation coefficients for E_- and E_+; s and s' scattering coefficients for E_s contributing to E_- and E_+, respectively; σ backscattering; w, v and u diffusion coefficients contributing to E_o.

This equations system can be represented in the vector–matrix notation as:

$$\frac{d}{dx}(E) = ME \tag{2}$$

E is the flux vector and M is the coefficients matrix. A general solution for canopy outward fluxes (E_{out}) can be found as function of incoming fluxes (E_{in}) and a diffusion matrix (Z):

$$\underbrace{\begin{bmatrix}E_s(-1)\\ E_-(-1)\\ E_+(0)\\ E_o(0)\end{bmatrix}}_{E_{out}} = \underbrace{\begin{bmatrix}\tau_{ss} & 0 & 0 & 0\\ \tau_{sd} & \tau_{dd} & \rho_{dd} & 0\\ \rho_{sd} & \rho_{dd} & \tau_{dd} & 0\\ \rho_{so} & \rho_{do} & \tau_{do} & \tau_{oo}\end{bmatrix}}_{Z} \underbrace{\begin{bmatrix}E_s(0)\\ E_-(0)\\ E_+(-1)\\ E_o(-1)\end{bmatrix}}_{E_{in}} \tag{3}$$

where (-1) corresponds to canopy bottom and (0) canopy top. Sub-indices for solar (s), diffuse (d) and in the observer direction (o) fluxes are added to transmittance (τ) and reflectance (ρ) coefficients. For the computation of canopy directional reflectance, the system can be expressed in subvectors and submatrixes for downward (d) and upward (u) fluxes at the bottom (b) and top of canopy (t).

$$\begin{aligned}E^d &= \begin{bmatrix}E_s\\ E_-\end{bmatrix}, \qquad E^u = \begin{bmatrix}E_+\\ E_o\end{bmatrix},\\ T_d &= \begin{bmatrix}\tau_{ss} & 0\\ \tau_{sd} & \tau_{dd}\end{bmatrix}, \quad R_b = \begin{bmatrix}0 & 0\\ \rho_{dd} & 0\end{bmatrix},\\ R_t &= \begin{bmatrix}\rho_{sd} & \rho_{dd}\\ \rho_{so} & \rho_{do}\end{bmatrix}, \quad T_u = \begin{bmatrix}\tau_{dd} & 0\\ \tau_{do} & \tau_{oo}\end{bmatrix},\end{aligned} \tag{4}$$

Providing a border condition at canopy bottom an additional equation represents soil reflectance:

$$E^u(-1) = R_s E^d(-1) \tag{5}$$

where R_s is the matrix soil reflectance.

Eq. (4) can thus be written as:

$$\begin{aligned}E^d(-1) &= T_d E^d(0) + R_b E^u(-1)\\ E^u(0) &= R_t E^d(0) + T_u E^u(-1)\end{aligned} \tag{6}$$

thus expressing the reflected flux vector $E^u(0)$ at canopy top as function of incident $E^d(0)$:

$$E^u(0) = R_t^* E^d(0) \tag{7}$$

being R_t^* the top of canopy reflectance matrix defined as:

$$R_t^* = R_t + T_u(I - R_s R_b)^{-1} R_s T_d = \begin{bmatrix} \rho(\theta_s) & \rho \\ \rho(\theta_s, \theta_o, \varphi) & \rho(\theta_o) \end{bmatrix} \quad (8)$$

where $\rho(\theta_s)$ is the hemispherical reflectance for direct incidence, ρ is the hemispherical reflectance for hemispherical incidence, $\rho(\theta_s,\theta_o,\varphi)$ is the bi-directional reflectance and $\rho(\theta_o)$ is the directional reflectance for hemispherical incidence (see Verhoef, 1984, 1985). Relative azimuth angle φ is the difference between the incident azimuth angle and the observer direction azimuth angle.

Elements from scattering matrix (τ and ρ coefficients from Eq. (3)) are computed from canopy structure (*LAI*, leaf angle distribution, *hotspot* parameter and leaf optical properties), soil optical properties and geometric configuration. Computation of reflectance is made assuming that canopy is an homogeneous horizontal and infinitely extended layer composed by small and flat leaves.

2. *SAILHFlood* model

SAILHFlood is composed of stacked horizontal layers. Soil bottom layer reflection is considered lambertian. Above it there is a layer of submerged vegetation, where the energy propagation medium is water. Top layer consists of the portion of the emergent vegetation, the so called emerged vegetation. Air–water interface is not considered as a layer, because of its negligible thickness, although its effect is directly associated to change in fluxes direction. The surface water is considered as an interface that interacts with energy fluxes by changing their direction due to the difference in refractive rates of both media. To compute submerged vegetation reflectance the coefficients of Duntley equations were modified by adding water optical properties. Air–water interface reflectance was estimated by computing reflectance and transmittance coefficients at the level of the general solution of system.

Emerged vegetation reflectance is computed by the *SAILH* model (see Verhoef, 1984, 1985). Interface reflectance matrix is considered as the background reflectance matrix, since downward incoming radiation is reflected by soil and transmitted upward by submerged vegetation and interface. The *LAI* used to calculate the coefficients that provide solution to the radiative transfer equation applies only to emerged *LAI*.

Downward diffuse and direct radiation fluxes are transmitted by the emerged vegetation layer and intercepted by the submerged vegetation layer. Submerged vegetation reflectance is computed taking soil optical properties as background and τ and ρ scattering coefficients are affected by water optical properties.

From an additive method (van de Hulst, 1981; Cooper et al., 1982) it is possible to compute top of canopy reflectance as the sum of multiple layers and soil reflectance after a number of interaction between layers (Kallel et al., 2007, see Eq. (8)). Following this procedure, *SAILHFlood* model computes top of flooded canopy reflectance considering emerged vegetation layer (*VE*), air–water interface (*I*), submerged vegetation layer (*VS*) and soil (*S*):

$$\begin{aligned} R_t^{VS+S} &= R_t^{VS} + T_u^{VS}(I - R_t^S R_b^{VS})^{-1} R_t^S T_d^{VS} \\ R_t^{I+VS+S} &= R_t^I + T_u^I(I - R_t^{VS+S} R_b^I)^{-1} R_t^{VS+S} T_d^I \\ R_t^{VE+I+VS+S} &= R_t^{VE} + T_u^{VE}(I - R_t^{I+VS+S} R_b^{VE})^{-1} R_t^{I+VS+S} T_d^{VE} \end{aligned} \quad (9)$$

where R_t^{VS+S} represents submerged vegetation reflectance matrix, considering underlying soil; R_t^{I+VS+S} represents interface reflectance matrix, taking into account submerged vegetation and soil underlying layers; and $R_t^{VR+I+VS+S}$ represents emerged vegetation reflectance matrix, considering all underlying layers and top of canopy reflectance.

Elements of top and bottom reflectance matrices (R_t and R_b, respectively) and upward and downward fluxes transmittance matrices (T^u and T^d, respectively) follow the definition made in Eq. (4). Coefficients and fluxes interactions are schematically represented in Fig. 1.

2.1. Air–water interface

Transmission of energy through the interface depends on the flux direction as the change of propagation medium from air to water and *vice versa* changes direction of lightwave propagation. Reflectance and transmittance matrices are defined in Eq. (10).

$$\begin{aligned} T_d^I &= \begin{bmatrix} \tau_{d_{ss}}^I & \tau_{d_{ds}}^I \\ \tau_{d_{sd}}^I & \tau_{d_{dd}}^I \end{bmatrix}, \quad R_t^I = \begin{bmatrix} \rho_{t_{sd}}^I & \rho_{t_{dd}}^I \\ \rho_{t_{so}}^I & \rho_{t_{do}}^I \end{bmatrix}, \\ T_u^I &= \begin{bmatrix} \tau_{u_{dd}}^I & \tau_{u_{od}}^I \\ \tau_{u_{do}}^I & \tau_{u_{oo}}^I \end{bmatrix}, \quad R_b^I = \begin{bmatrix} \rho_{b_{ds}}^I & \rho_{b_{os}}^I \\ \rho_{b_{dd}}^I & \rho_{b_{od}}^I \end{bmatrix}, \end{aligned} \quad (10)$$

2.1.1. Downward fluxes coefficients

Fresnel laws predict the proportion of radiation traversing an interface between two isotropic media. Incident flux is both reflected (R) or transmitted (T) and each magnitude depends on polarization of incident flux (Landau and Lifshitz, 1984). If polarization is perpendicular to the incident plane, reflection coefficient (R) is computed as:

$$R_\perp = \left[\frac{\sin(\theta_t - \theta_t)}{\sin(\theta_t + \theta_t)}\right]^2 \quad (11)$$

where θ_i and θ_t are incident and transmitted zenith angles, respectively. On the other way, if polarization is parallel to the incident plane, reflection coefficient ($R_{||}$) is computed as:

$$R_{||} = \left[\frac{\tan(\theta_t - \theta_t)}{\tan(\theta_t + \theta_t)}\right]^2 \quad (12)$$

Incident angle (θ_i) is given by solar angle (θ_s), and transmitted angle (θ_t) in the water which differs by the phenomena of diffraction from that in air (θ_s). It is calculated from Snell's law and using the water refraction index for each wavelength, and denoted from now on as θ_s^w.

In the specular case in which the observation angle (θ_o) equals the solar lightwave incidence angle (θ_s), the interface bidirectional reflectance ($\rho_{t_{so}}^I$) is calculated as the average of reflection coefficients of both polarizations. In the case that the observation angle (θ_o) differs from the solar angle (θ_s), the fraction of solar radiation reflected to observer direction is considered negligible, due a flat water surface is assumed, hence interface bidirectional reflectance ($\rho_{t_{so}}^I$) equals 0 and all reflected radiation is ascribed to the hemispherical component ($\rho_{t_{sd}}^I$) of both polarization (Eqs. (11) and (12)):

$$\begin{matrix} \theta_o = \theta_s & \rho_{t_{so}}^I \\ \theta_o \neq \theta_s & \rho_{t_{sd}}^I \end{matrix} = 0.5 \left\{ \left[\frac{\sin(\theta_s - \theta_s^w)}{\sin(\theta_s + \theta_s^w)}\right]^2 + \left[\frac{\tan(\theta_s - \theta_s^w)}{\tan(\theta_s + \theta_s^w)}\right]^2 \right\} \quad (13)$$

where the 0.5 factor stands for an equal parts average of both polarization components. Reflectance coefficients given in Eq. (13), as well as those given from now on, are not expressed as the classical reflectance factors found in literature for an incident radiance with

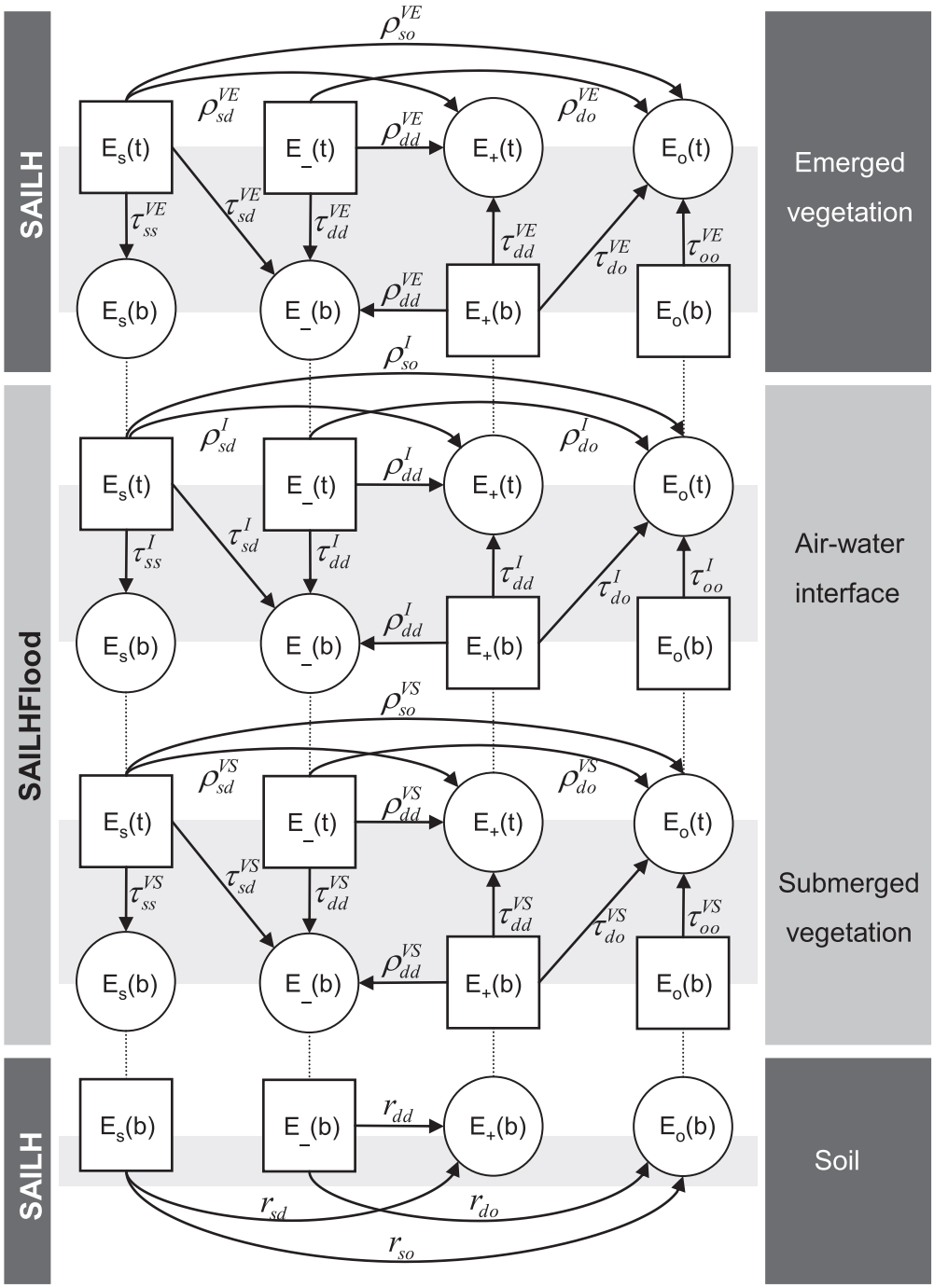

Fig. 1. Downward and upward radiation fluxes interact with the combination of soil, submerged vegetation and emerged vegetation layer of *SAILHFlood* model. Squares and circles represent incidents and outwards fluxes, respectively (E_o direct solar irradiance, E_- diffuse downward irradiance, E_+ diffuse upward irradiance, E_o radiance in the observer radiation). Reflectance (ρ) and transmittance (τ) coefficients show fluxes interactions. Sub-indices indicate incident and outward flux type: direct solar (s) or in the observer direction (o), or diffuse (d). Soil reflectance coefficients are denoted by *r*. Modified from Beget et al. (2010).

a given solid angle but instead they are only the fraction of the radiance from a single zenit angle. It is straightforward to accommodate all reflectances and transmitances presented henceforth in a compatible manner with the expressions with a defined solid angle for the corresponding radiance as in classical reflectance factors. Then directional transmittance ($\tau^I_{d_{ss}}$) is:

$$\tau^I_{d_{ss}} = 1 - \rho^I_{t_{sd}} \tag{14}$$

As the water–air interface is assumed to be steady, that is, no wind creates ripples that scatter radiation in directions not given by the Snell law, directional–hemispherical transmittance ($\tau^I_{d_{sd}}$) and hemispherical–directional transmittance ($\tau^I_{d_{ds}}$) are assumed nil. Bi-hemispherical reflectance ($\rho^I_{t_{dd}}$) is computed as an average on the hemisphere of the Fresnel reflection coefficient for both polarizations (Eq. (13)) of diffuse radiation incident in the interface assumed to be isotropic. In this case it has no dependence on the azimuthal

angle (π) and the averaging (Eq. (15)) is thus made over all possible polar incidence angles (θ, 0 to $\pi/2$):

$$\rho^I_{t_{dd}} = \frac{1}{2\pi}\int_0^{2\pi}\left\{\int_0^{\pi/2} 0.5\left[\left[\frac{\sin(\theta-\arcsin(\sin\theta/\eta_w))}{\sin(\theta+\arcsin(\sin\theta/\eta_w))}\right]^2+\left[\frac{\tan(\theta-\arcsin(\sin\theta/\eta_w))}{\tan(\theta+\arcsin(\sin\theta/\eta_w))}\right]^2\right]d\theta\,\sin\theta\right\}d\varphi$$
$$= 0.5\int_0^{\pi/2}\left\{\left[\frac{\sin(\theta-\arcsin(\sin\theta/\eta_w))}{\sin(\theta+\arcsin(\sin\theta/\eta_w))}\right]^2+\left[\frac{\tan(\theta-\arcsin(\sin\theta/\eta_w))}{\tan(\theta+\arcsin(\sin\theta/\eta_w))}\right]^2\right\}d\theta\sin\theta \quad (15)$$

being η_w the water refractive index. Finally, bi-hemispherical transmittance ($\tau^I_{d_{dd}}$) is given by:

$$\tau^I_{d_{dd}} = 1-\rho^I_{t_{dd}} \quad (16)$$

2.1.2. Upward fluxes coefficients

When radiation goes from a medium with higher refraction index to one with a lower one – such as from water to air – total internal reflection occurs if zenith angle of incident flux is higher or equal to critical angle ($\theta_i \geq \theta_c$), so energy is totally reflected back. The critical angle is the value for θ_i for which $\theta_t = 90^\circ$ and is given by:

$$\sin\theta_c = \frac{\eta_t}{\eta_t} \quad (17)$$

being η_t the refractive index for air and η_i the refractive index for water.

Thus, if the underwater zenith observation angle (θ^w_o) is greater than the critical angle, total internal reflection occurs and coefficients of directional-hemispherical ($\rho^I_{b_{od}}$) is equal to 1.

On the opposite case when $\theta_w < \theta_c$ the coefficient $\rho^I_{b_{od}}$ should be computed as the average of Fresnel coefficients $R_\perp$ and $R_{||}$, in this case $\theta_i = \theta_w$ and $\theta_t = \theta_o$:

$$\rho^I_{b_{od}} = 0.5\left\{\left[\frac{\sin(\theta^w_o-\theta_o)}{\sin(\theta^w_o+\theta_o)}\right]^2+\left[\frac{\tan(\theta^w_o-\theta_o)}{\tan(\theta^w_o+\theta_o)}\right]^2\right\} \quad (18)$$

To evaluate bi-hemispherical reflectance $\rho^I_{b_{dd}}$ an averaging over θ_w from 0 to $\pi/2$ of Eq. (18) is performed in the same fashion as done for obtaining Eq. (15). However each of the Fresnel terms in Eq. (18) should be squared in the correct mathematical fashion for the complex values they deliver for any θ^w_o exceeding the θ_o to produce a reflectance equal to 1. To do that it suffices with multiplying each term by its complex conjugate or taking the absolute value of each term before squaring it as shown in Eq. (19):

$$\rho^I_{b_{dd}} = \frac{1}{2\pi}\int_0^{2\pi}\left\{\int_0^{\pi/2} 0.5\left[\left|\frac{\sin(\theta_w-\arcsin(\eta_w\sin\theta_w))}{\sin(\theta_w+\arcsin(\eta_w\sin\theta_w))}\right|^2+\left|\frac{\tan(\theta_w-\arcsin(\eta_w\sin\theta_w))}{\tan(\theta_w+\arcsin(\eta_w\sin\theta_w))}\right|^2\right]\text{sen}\,\theta_w\,d\theta_w\right\}d\varphi$$
$$= 0.5\int_0^{\pi/2}\left[\left|\frac{\sin(\theta_w-\arcsin(\eta_w\sin\theta_w))}{\sin(\theta_w+\arcsin(\eta_w\sin\theta_w))}\right|^2+\left|\frac{\tan(\theta_w-\arcsin(\eta_w\sin\theta_w))}{\tan(\theta_w+\arcsin(\eta_w\sin\theta_w))}\right|^2\right]\text{sen}\,\theta_w\,d\theta_w \quad (19)$$

Bi-hemispherical ($\tau^I_{u_{dd}}$) and bi-directional transmittance ($\tau^I_{u_{oo}}$) are given respectively by:

$$\tau^I_{u_{dd}} = 1-\rho^I_{b_{dd}}$$
$$\tau^I_{u_{oo}} = 1-\rho^I_{b_{od}} \quad (20)$$

Then hemispherical–directional ($\tau^I_{u_{do}}$) and directional–hemispherical ($\tau^I_{u_{od}}$) transmittance are considered symmetric and both equal to 0.

Finally, hemispherical–directional ($\rho^I_{b_{ds}}$) and bi-directional reflectance ($\rho^I_{b_{os}}$) are equal to 0, because as done in *SAILH* model, it is considered that the contribution to radiation fluxes after multiple scatterings can be neglected (Verhoef, 1985).

2.2. Submerged vegetation reflectance

Radiative transfer equation for submerged canopy is represented by Duntley differential equations in the same way the *SAILH* does for land vegetation. Its coefficients take into account extinction, scattering and attenuation produced by vegetation tissues and water. Each coefficient with a sub-index "sum", is computed as the algebraic sum of *SAILH* coefficient and a coefficient that accounts for the attenuation caused by water. *SAILH* coefficients, with the sub-index "veg" are computed from submerged *LAI* fraction. Once Duntley submerged coefficients have been computed they are applied to *SAILH* for computation of general solution.

Scattering and absorption process affects light propagation in water. Light can be scattered by water itself and by the suspended particles (Smith and Baker, 1981). In our model it is assumed that vegetation submerged into clear water without suspended particles.

2.2.1. Extinction coefficient for solar flux k

The extinction coefficient for solar flux (E_s) is calculated as the sum of absorption (α_w) and scattering (β_w, Fig. 2) in optical path and direction θ^s_w. Absorption coefficient was calculated as the average from measured coefficients by different authors in multiple spectral ranges (Table 1). Spectral data was taken from a compendium of water optical properties made by Scott Prahl (available at http://omlc.ogi.edu/spectra/water/abs/index.html, September 29th, 2008). Available values from α_w were averaged for each wavelength from 400 to 2400 nm. Data at higher spectral resolution was interpolated to 1 nm resolution.

The extinction coefficient for water (k_w) is defined as:

$$k_w = \frac{1}{\cos\theta^w_s}(\alpha_w+\beta_w) \quad (21)$$

Scattering processes between 400 and 800 nm are assumed to be perfectly elastic, meaning that fluxes only change direction and do not lose intensity; and for wavelengths higher than 800 nm is close to zero (Smith and Baker, 1981). To compute β_w for the entire range of the spectrum data was adjusted and the following function was obtained: $\beta_w = 1.37\times10^9\lambda^{-4.328}+3.111\times10^{-5}$, were λ is wavelength in nanometers.

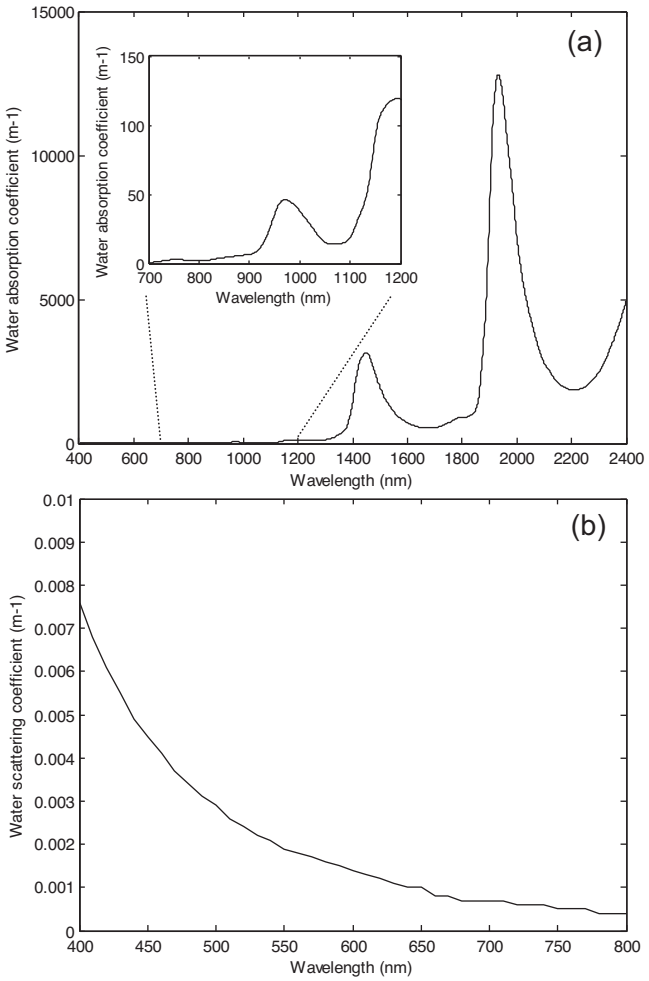

Fig. 2. (a) Water absorption coefficient (α_w) (m^{-1}) calculated as the average of coefficients measured by different authors (see Table 1). (b) Water scattering coefficient (β_w) (m^{-1}) taken from Smith and Baker (1981) for 400 to 800 nm range.

Finally, the extinction coefficient for submerged canopy layer (k_{sum}) is that due to the vegetation (k_{veg}) with the addition of that due to water (k_w):

$$k_{sum} = k_{veg} + k_w \tag{22}$$

where k_{veg} is computed by the standard *SAILH* model (Verhoef, 1984).

2.2.2. Forwardscattering and backscattering solar flux coefficients

Forward and backward scattering are considered equiprobable processes. Forwardscattering (s_{sum}) and backscattering (s'_{sum}) coefficients are computed as:

$$s_w = 0.5\frac{1}{\cos\theta_s^w}\beta_w \qquad s'_w = 0.5\frac{1}{\cos\theta_s^w}\beta_w \tag{23}$$

Both s_{sum} and s'_{sum} account for scattering of solar flux (E_s) where $1/\cos\theta_s^w$ is the light path in the water, and the 0.5 factor accounts for the probability for upward and downward scattering. Finally, the contribution of E_s to diffuse fluxes (E_- and E_+) is due to submerged leaves and water (Rayleigh scattering). Thus scattering coefficients for submerged canopy are calculated as:

$$S_{sum} = S_{veg} + S_w \qquad S'_{sum} = S'_{veg} + S'_w \tag{24}$$

Table 1
References and spectral ranges considered for α_w computation.

Reference	Spectral range (nm)
Boivan et al. (1986)	400–578
Buiteveld et al. (1994)	400–800
Hale and Querry (1973)	400–2400
Kopelevich (1976)	400–600
Kou et al. (1993)	667–2400
Morel and Prieur (1977)	400–700
Palmer and Williams (1974)	690–2400
Pope and Fry (1997)	400–727
Segelstein (1981)	400–2400
Smith and Baker (1981)	400–800
Sogandares and Fry (1997)	400–640
Sullivan (1963)	400–450
Wieliczka et al. (1989)	801–790
	1232–2400

where S_{veg} and S'_{veg} are calculated by *SAILH* model (Verhoef, 1984).

2.2.3. Scattering diffuse flux coefficients

The coefficients σ_{sum} and σ'_{sum} describe the scattered proportion of diffuse fluxes (E_- and E_+) due to submerged canopy. For water, backscatter and forwardscattering coefficients are obtained through integration over all the range for θ_s^w, considering it symmetrical in azimuth(φ) and equal probability of occurrence of upward and downward scattering (factor 0.5):

$$\sigma_w = \frac{1}{2\pi(1-\cos\theta_c)}\int_0^{2\pi}\int_0^{\theta_c}\sin\theta_s^w\frac{h}{\cos\theta_s^w}d\theta_s^w d\varphi\beta_w = \frac{0.5h}{1-\cos\theta_c}\int_0^{\theta_c}\tan\theta_s^w\, d\theta_s^w\beta_w \tag{25}$$

Backscatter coefficient of diffuse fluxes due to vegetation (σ_{veg}) is computed by *SAILH* model (Verhoef, 1984). So finally the backscatter by the submerged vegetation layer is:

$$\sigma_{sum} = \sigma_{veg} + \sigma_w \tag{26}$$

2.2.4. Attenuation coefficient of diffuse fluxes

In the same way as σ_{sum}, attenuation coefficient of diffuse fluxes in water (a_{sum}) is computed from sphere integration of θ_s^w. Attenuation is caused by absorption and scattering processes in visible wavelength, but in infrared wavelength range the attenuation is caused only by absorption. As explained previously scattering becomes 0 over wavelengths longer than 800 nm. A half of the flux is backscattered so it is not involved in attenuation processes:

$$a_w = \frac{\int_0^{\theta_c} h\tan\theta_s^w d\theta_s^w}{\int_0^{\theta_c}\sin\theta_s^w d\theta_s^w}(\alpha_w + 0.5\beta_w) \tag{27}$$

Thus total attenuation is given by:

$$a_{sum} = a_{veg} + a_w \tag{28}$$

where a_{veg} is attenuation coefficient due to vegetation computed by *SAILH* model (Verhoef, 1984).

2.2.5. Extinction coefficient of direct flux in observer direction

Similarly to the computation of extinction coefficient for downward direct flux, the extinction coefficient of direct flux in observer direction (K_w) is calculated as:

$$K_w = \frac{h}{\cos\theta_o^w}(\alpha_w + \beta_w) \tag{29}$$

where zenithal observation angle (θ_o^w) is computed following Snell's law:

$$\theta_o^w = \arcsin\left(\frac{\sin\theta_o}{\eta_w}\right) \tag{30}$$

Then, total extinction coefficient of direct flux in observer direction for submerged canopy (K_{sum}) is given by water extinction coefficient (K_w) and vegetation extinction coefficient (K_{veg}):

$$K_{sum} = K_{veg} + K_w \tag{31}$$

2.2.6. Diffusion coefficients contributing to observer direction flux

The coefficients for downward and upward diffuse fluxes (v_{sum} and u_{sum}, respectively), are calculated by *SAILH* model (Verhoef, 1984):

$$\begin{aligned} v_{sum} &= \left(\frac{ref + tran}{2}\right) K_{sum} + \left(\frac{ref - tran}{2}\right) \delta_{LAIsum} \cos^2\bar{\theta}_l \\ u_{sum} &= \left(\frac{ref + tran}{2}\right) K_{sum} - \left(\frac{ref - tran}{2}\right) \delta_{LAIsum} \cos^2\bar{\theta}_l \end{aligned} \tag{32}$$

where δ_{LAIsum} is leaf area density and is calculated as the ratio of the submerged LAI (LAI_{sum}) to the relative frequency of leaf inclination angle θ_l; *ref* and *tran* are leaf reflectance and transmittance respectively; and $\bar{\theta}_l$ is average leaf inclination angle.

Bi-directional scattering coefficient (w_{sum}) is calculated from *SAILH* model (Verhoef, 1984) as:

$$\begin{aligned} w_{sum} = \frac{\delta_{LAFsum}}{2\pi}&[\pi ref - \beta_2^w(ref + tran)](2\cos^2\overline{\theta_l} \\ &+ \sin^2\overline{\theta_l}\tan\theta_s^w\tan\theta_o^w\cos\psi) + (ref + tran)\mathrm{sen}\beta_2^w \\ &\times\left[\frac{2\cos^2\overline{\theta_l}}{\beta_s^w\cos\beta_o^w} + \cos\beta_1^w\cos\beta_2^w\sin\overline{\theta_l}\tan\theta_s^w\tan\theta_o^w\right] \end{aligned} \tag{33}$$

where β_o^w and β_s^w are transition angles (Verhoef, 1984); β_1^w, β_2^w and β_3^w are auxiliary azimuthal angles below water; and ψ is relative azimuthal angle between sun and observer.

Having obtained the coefficients for the Duntley differential equation system that allows to describe fluxes at the submerged vegetation layer, the diffusion matrix for this layer can be obtained as a solution for this system. The reflectance (ρ^{VS}) and transmittance (τ^{VS}) coefficients for the submerged vegetation layer diffusion matrix are defined as:

$$\begin{aligned} T_d^{VS} &= \begin{bmatrix} \tau_{d_{ss}}^{VS} & \tau_{d_{ds}}^{VS} \\ \tau_{d_{sd}}^{VS} & \tau_{d_{dd}}^{VS} \end{bmatrix}, \quad R_t^{VS} = \begin{bmatrix} \rho_{t_{sd}}^{VS} & \rho_{t_{dd}}^{VS} \\ \rho_{t_{so}}^{VS} & \rho_{t_{do}}^{VS} \end{bmatrix}, \\ T_u^{VS} &= \begin{bmatrix} \tau_{u_{dd}}^{VS} & \tau_{u_{od}}^{VS} \\ \tau_{u_{do}}^{VS} & \tau_{u_{oo}}^{VS} \end{bmatrix}, \quad R_b^{VS} = \begin{bmatrix} \rho_{t_{ds}}^{VS} & \rho_{t_{os}}^{VS} \\ \rho_{t_{dd}}^{VS} & \rho_{t_{od}}^{VS} \end{bmatrix}, \end{aligned} \tag{34}$$

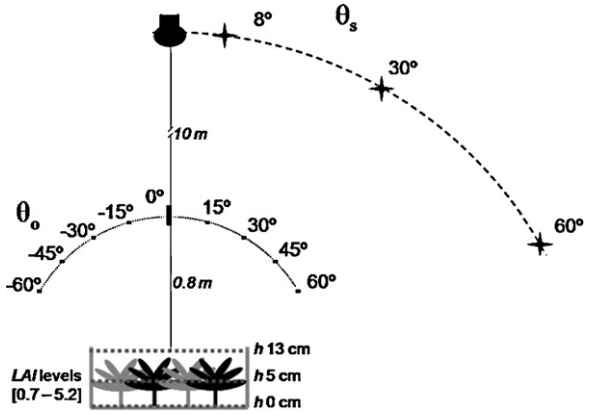

Fig. 3. Schematic representation of experiment. Illumination zenith angles (θ_s), viewing zenith angles (θ_o), water levels (h) are represented. For each LAI level [0.7 1.2 1.7 3.5 5.2] three θ_s, nine θ_o and three h were tested.

3. Test model

Hyperspectral reflectance measurements of artificially flooded canopies of *Pittosporum tobira* (Thunb.) W.T. Aiton in transparent containers provide experimental data (Beget, 2009) to evaluate the model. In the experiment several measurements were performed for different leaf area indices, water depth and geometrical configuration (Table 2 and Fig. 3). Five different canopy densities were generated covering a wide range of *LAI* (0.7–5.2) planting increasing density of shoots over a brown painted plate. Reflectance measurements were made for three flooding conditions: in canopies without water, with an intermediate level of water (5 cm) and with the canopy totally submerged (13 cm of water). In all cases three incidence angles (θ_s = [8° 30° 60°]) were tested for 9 viewing zenith angles (θ_o = [−60° −45° −30° −15° 0° 15° 30° 45° 60°]) always in the principal plane (relative azimuth angle, $\varphi_s - \varphi_o = 0°$).

Table 2
Experiment variables that were later used as inputs for the numerical simulation for comparison.

SAILHFlood input variables	Symbol	Units/range	Cases
Water level	h	meters	[0 0.05 0.13]
Emerged *LAI*	LAI_{em}	m^2/m^2	$[0.7\ 1.2\ 1.7\ 3.5\ 5.2]_{h=0}[0.61\ 1.05\ 1.48\ 3.06\ 4.54]_{h=0.05}[0.01\ 0.01\ 0.02\ 0.03\ 0.05]_{h=0.13}$
Submerged *LAI*	LAI_{sum}	m^2/m^2	$[0\ 0\ 0\ 0\ 0]_{h=0}$ $[0.089\ 0.15\ 0.22\ 0.44\ 0.66]_{h=0.05}$ $[0.69\ 1.19\ 1.68\ 3.47\ 5.15]_{h=0.13}$
Average leaf angle inclination	$\bar{\theta}_l$	degrees	39[a]
Hotspot	*hot*	–	0.42[a]
Leaf reflectance	*refl*	0–1	[a]
Leaf transmittance	*tran*	0–1	[a]
Solar zenith angle	θ_s	degrees	[8 30 60]
Viewing zenith angle	θ_o	degrees	[−60 −45 −30 −15 0 15 30 45 60]
Azimuthal relative angle	ψ	degrees	0[a]
Diffuse radiation factor	*skyl*	0–1	0[a]
Soil bidirectional reflectance	r_{os}	0–1	[a]
Soil bi-hemispherical reflectance	r_{dd}	0–1	[a]
Soil directional-hemispherical reflectance	r_{sd}	0–1	[a]
Soil hemispherical-directional reflectance	r_{do}	0–1	[a]

[a] Unchanged between measurements.

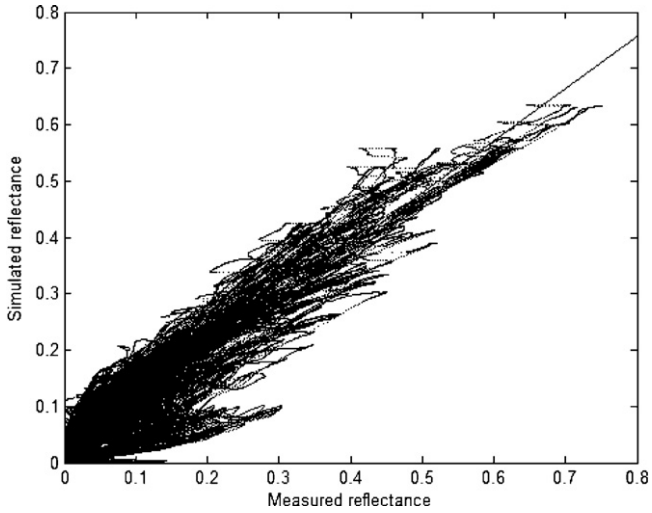

Fig. 4. Comparison between simulated by *SAILHFlood* and measured reflectance for hyperspectral bands (400–2400 nm) bands. Least squares linear fit. $R^2 = 0.9075$. Average *RMSE* = 0.0355.

The experiment were performed indoor using a 2000 W halogen projector plugged into a stabilized power source and placed at 10–15 m from the 'canopies' to get better collimated light beam over the sampled area (Fig. 3). Reflectance measurements were acquired with an ASDFieldSpec© spectroradiometer equipped with a 8° FOV lens in the 400–2400 nm range with a 1 nm of spectral sampling interval. Calibrations were made frequently using a Spectralon Labsphere® reference panel to get absolute reflectance values.

Measured data were filtered through counting errors at the acquisition process. Specular situations ([8°, −15°], [30°, −30°] and [60°, −60°]) and a particular situation when sensor shadowed the sample ([8°, 15°], [30°, 30°], [60°, 60°]) were eliminated from data pool.

A plot of all reflectivity measurements against modeled ones show that simulated data matches qualitatively well measured data (Fig. 4, $f(x) = p1 \times x + p2$; coefficients (with 95% confidence bounds): $p1 = 0.9275$ (0.9266, 0.9285), $p2 = 0.01645$ (0.01632, 0.01659).

In order to provide a quantitative comparison of similarity in the magnitude of reflectance, root mean squared error (*RMSE*, Eq. (35)) between simulation and measurement is calculated as:

$$RMSE = \sqrt{\frac{1}{N}\sum_{i=0}^{N-1}\left(\overline{R_{isim}} - R_{imeas}\right)^2} \tag{35}$$

where R_{isim} and R_{imeas} are simulated and measured reflectance respectively, and N the sampled spectral bands.

Comparison was also performed in terms of spectral angle as a measure of similarity in the shape of spectra (Debba et al., 2005). The spectral angle (*SA*) between two spectra is the difference angle between two vectors in m-dimensional space, where m in our case stands for the number of available spectral bands. The spectral angle is calculated in radians as:

$$SA = \cos^{-1}\left(\frac{sim(\lambda)\cdot meas(\lambda)}{\left\|sim(\lambda)\right\|\cdot\left\|meas(\lambda)\right\|}\right) \tag{36}$$

where λ is the wavelength range for m band, and $sim(\lambda)$ and $meas(\lambda)$ are simulated and measured spectra respectively.

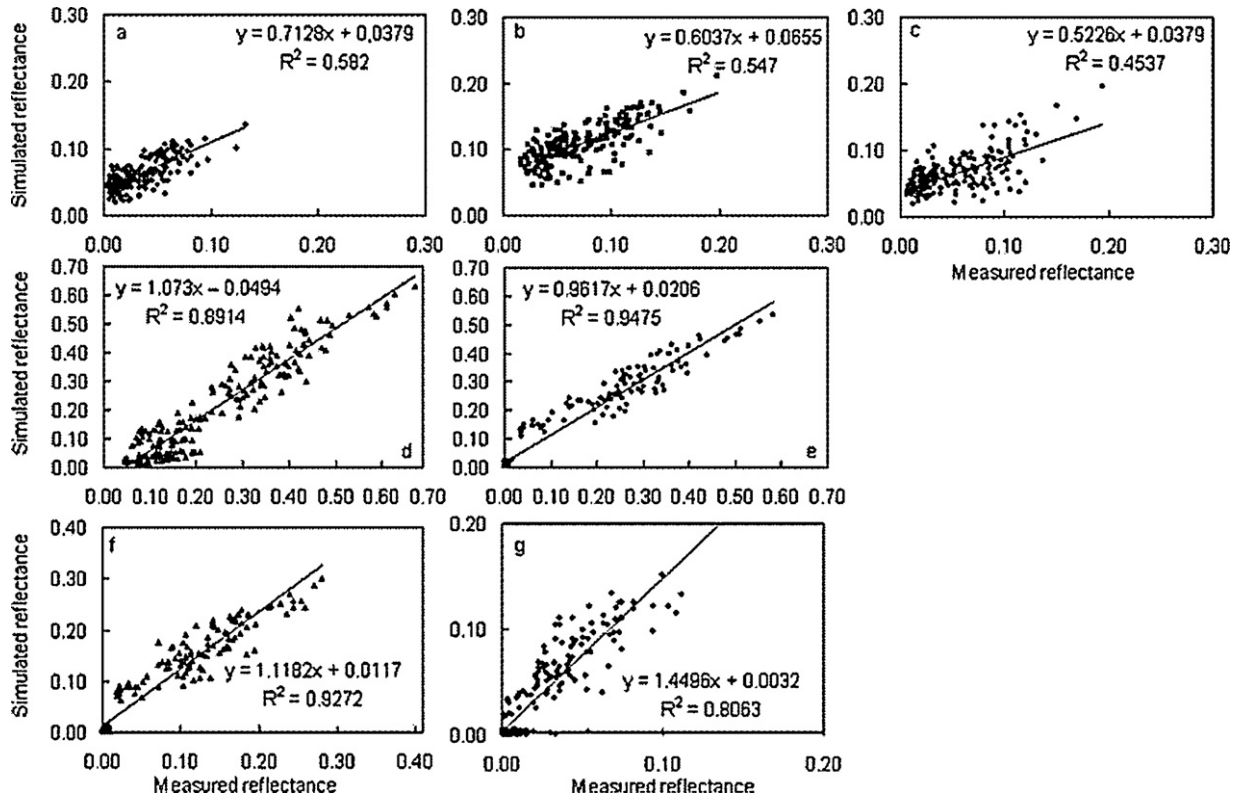

Fig. 5. Comparison between simulated by *SAILHFlood* and measured reflectance for *MODIS* bands (a: 459–479 nm, b: 545–565 nm, c: 620–670 nm, d: 841–876 nm, e: 1230–1250 nm, f: 1628–1652 nm, g: 2105–2155 nm). Spectral response for *MODIS* bands were calculated from averaging hyperspectral data.

4. Model performance results

4.1. Model performance for hyperspectral measurements

The averaged *RMSE* obtained for hyperspectral bands was 0.0355, and the spectral angle *SA* was 0.2591 radians. The correlation (95%) and *RMSE* obtained between simulated and observed data are comparable with those obtained by other authors (Jacquemoud and Baret, 1990; Jacquemoud et al., 2000). In general, simulated reflectance showed a greater similarity in terms of magnitude than spectral shape. Although several authors used *SA* as a methodology to compare spectra in satellite images classification or inversion of modeled non-flooded vegetation reflectance (Debba et al., 2005; Yebra Álvarez, 2008), we could not find in literature a threshold value to classify *SA*. Results indicated that the simulated spectra shows greater similarity to those observed in terms of shape: those for the partially submerged canopies and those without water (water level 5 and 0 cm respectively). No flooded situation also showed lower values of *RMSE*, resembling more the magnitude of spectra. In contrast, in the case of completely submerged canopies, the spectra were more similar in magnitude but variable in terms of similarity in shape.

Model performance in terms of *RMSE* was not sensitive to changes in leaf area index, observation and illumination zenith angles or water level. This is an important factor in favor of the inversion of this model to a diversity of flooded vegetation situations and available sensors.

4.2. Model performance for MODIS bands

Model performed better considering only *MODIS* sensor bands in terms of correlation (all data, $f(x) = p1 \times x + p2$; coefficients (with 95% confidence bounds): $p1 = 0.9128$ (0.8956, 0.93), $p2 = 0.02159$ (0.01914, 0.02404)). However, *RMSE* = 0.0364 and *SA* = 0.2753 did not vary largely. *SAILH* model simulated better spectral response in *MODIS* visible bands than *SAILHFlood* model, inverse results were found for infrared bands. Incorporation of water resulted in a decreasing of correlation coefficient for visible bands in 22% average and an increasing for infrared bands of 17% average.

In the case of *SAILHFlood* model a higher correlation between simulated and measured reflectance were found for near infrared and short-wave infrared bands (Fig. 5). Specifically, according to the values of relative *RMSE*, the bands that better estimated reflectance were near-infrared (841–876 nm) and the short-wave infrared (1230–1250 nm).

The directional component of simulated reflectance was stronger at visible and near infrared bands in the case of higher water depth and higher illumination angles (Fig. 6). In the case of partially submerged canopies upon an increase on illumination angle, the directional component is more evident in the hotspot direction as documented by other authors (*e.g.* Kuusk, 1985; Jacquemoud et al., 2000). However, our model currently does not take into consideration the hotspot situation, so no comparison for this case is valid. When canopies were totally submerged, reflectance slowly decreased in the nadir direction.

Errors in data collection could be responsible for a portion of lack of fit found for *SAILHFlood* data. Another possible source of error in estimations is that the *SAILH* do not differentiate coefficients of reflection and transmission of adaxial and abaxial leaf sides. In particular, leaves of *P. tobira* (Thunb.) W.T. Aiton showed slight differences in the magnitude of radiation reflected and transmitted by each side (not shown). In the model definition this variable was not introduced because it was considered important to maintain the relative simplicity of the model, to preserve the least possible

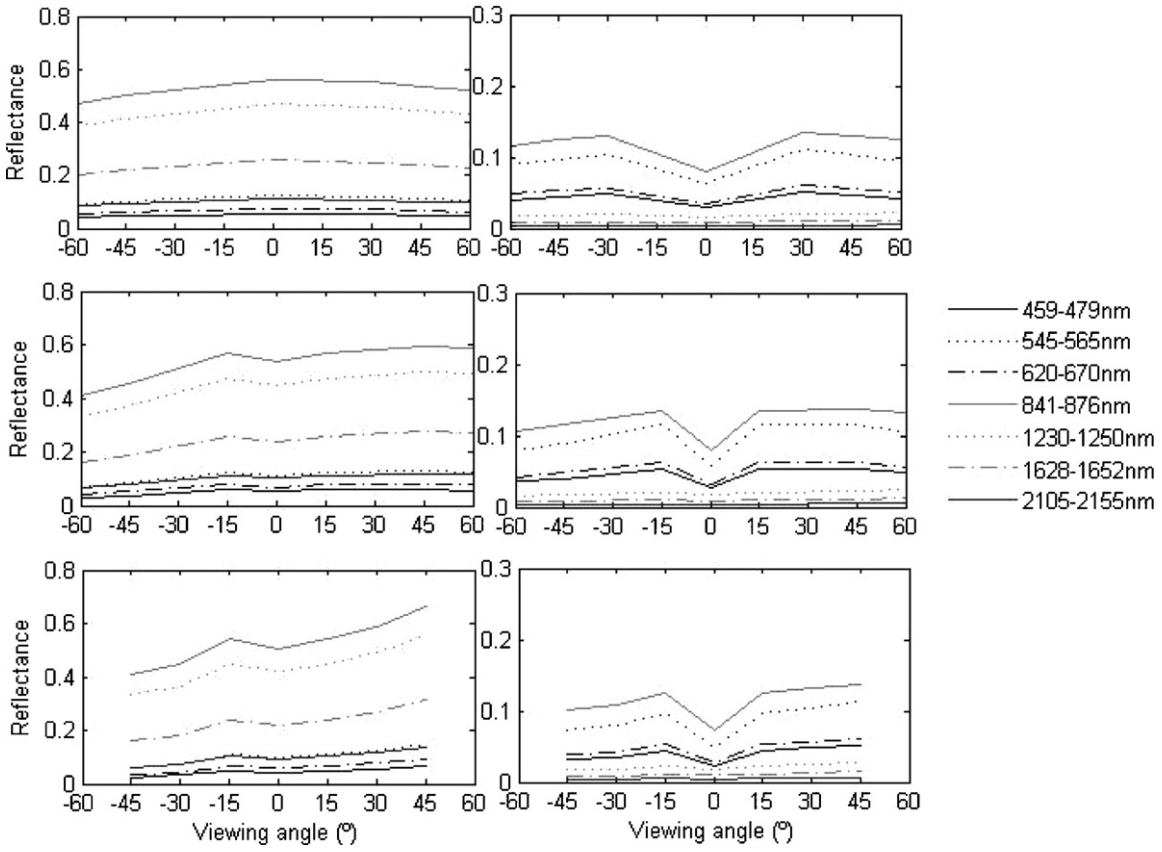

Fig. 6. Simulated reflectance at some measured viewing angles (°) on experimental for *MODIS* bands. At left 0.05 m water level, at right 0.13 m water levels. Rows correspond to illumination angles, from top to bottom 8°, 30° and 60°. Total *LAI* = 5.2. Specular situations are not represented.

number of variables. Also it must be taken into account the fact that *SAILHFlood* does not currently incorporate the effect of common scattering materials in the water. Anyway, the results obtained can be considered satisfactory, because, on average, the model estimated canopy reflectance with an error of 4%.

5. Conclusions

The *SAILHFlood* model extends the applicability of reflectance simulation models, such as *SAILH*, to plant environments with the presence of surface water. In these systems, water plays a dual role by modifying the emerged *LAI* and the substrate. The results found in this study allow inferring that flood modifies the spectral response through two mechanisms: reducing the leaf area that intercepts solar radiation and attenuating radiation transmitted by the canopy and reflected by the ground. This latter mechanism is the most influencing one on the reflectance registered at the top of canopy.

The model is useful to determine the more suitable wavelengths or spectral indices to study the different situations of flooded vegetation. The results showed that while the short wave infrared bands are strongly associated with water, as has been reported in the literature (*e.g.* Palmer and Williams, 1974; Smith and Baker, 1981), it is necessary to use them in combination with *NIR* to separate the effect of water in plant tissues (Sims and Gamon, 2003). These considerations are important when studying diverse situations. For example, rice crop water depth used in production management ranged from 5 to 10 cm, left a greater proportion of leaf area above it in the later stages of cycle, while in natural environments such as grasslands or marshes of the Parana River Delta these conditions may be more variable. We therefore believe that the model will be of great utility when choosing or designing the most appropriate sensor for each of the flooded areas.

As reviewed by Jacquemoud et al. (2009) *SAILH* model has been used in several applications in biophysical variables estimation from model inversion. Examples of this procedure include ground, airborne and spaceborne data. Model performance at *MODIS* bands are promising so it is expected that *SAILHFlood* model can be applied for studies of flooded environments.

The performance of the *SAILHFlood* model was assessed varying *LAI*, water depth and viewing and illumination angles. Results showed that the model would work for a wide range of situations. For example, the viewing angles tested, are consistent with those used most frequently by the currently available satellite sensors. Similarly, the model's performance was insensitive to changes in angle of illumination, water depth and *LAI*. These results make *SAILHFlood* applicable to a broad universe of measurement configurations, with the exception of situations in which the angles of illumination and observation are similar (specular positions).

As shown in this paper *MODIS* sensor images on board the Terra and Aqua satellites have a high potential to be used in conjunction with *SAILHFlood* model. Obtaining spatial information such as the water level and submerged and emerged *LAI*, in model inversion procedure, at a resolution of 6 ha, is an enormous challenge to achieve in future research. It will be useful for decision-making of ecologists, agronomists and all users of remote sensing in both: the production and the management of natural resources.

Acknowledgements

Authors are grateful to Jean-Francois Hanocq for his collaboration in spectral measurements performance. This work was supported by projects PICT 32415 (ANPCyT) and AERN4-AERN4642 (INTA) and by INRA EMMAH.

References

Andrieu, B., Baret, F., Jacquemoud, S., Malthus, T., Steven, M., 1997. Evaluation of an improved inversion of SAIL model for simulating bidirectional reflectance of sugar beet canopies. Remote Sensing of Environment 60, 247–257.

Baret, F., 1990. Factors and mechanism governing canopy spectral reflectance: application for Agriculture. Technical note.

Beget, M.E., 2009. Desarrollo y validación de un modelo de transferencia radiativa para vegetación inundada: SAILHFlood. Tesis para optar por el grado de Magister de la Universidad de Buenos Aires. Facultad de Agronomía, Universidad de Buenos Aires.

Beget, M.E., Di Bella, C.M., 2007. Flooding: the effect of water depth on the spectral response of grass canopies. Journal of Hydrology 335, 285–294.

Beget, M.E., Baret, F., Di Bella, C., Hanocq, J.F., 2010. Modelling reflectance of partially submerged canopies. 3rd International Symposium Recent Advances in Quantitative Remote Sensing. Torrent (Valencia, Spain) 27 September to 1 October 2010.

Bilge, F., Yazici, B., Dogeroglu, T., Ayday, C., 2003. Statistical evaluation of remotely sensed data for water quality monitoring. International Journal of Remote Sensing 24, 5317–5326.

Boivan, L.P., Davidson, W.F., Storey, R.S., Sinclair, D., Earle, E.D., 1986. Determination of the attenuation coefficients of visible and ultraviolet radiation in heavy water. Applied Optics 25, 877–882.

Buiteveld, H., Hakvoort, J.M.H., Donze, M., 1994. The optical properties of pure water. In: Jaffe, J.S. (Ed.), SPIE Proceedings on Ocean Optics XII, vol. 2258. , pp. 174–183.

Cooper, K., Smith, J.A., Pitts, D., 1982. Reflectance of a vegetation canopy using the adding method. Applied Optics 21 (22), 4112–4118.

Debba, P., van Ruitenbeek, F.J.A., van der Meer, F.D., Carranza, J.M., Stein, A., 2005. Optimal field sampling for targeting minerals using hyperspectral data. Remote Sensing of Environment 99, 373–386.

Guyot, G., Baret, F., Jacquemoud, S., 1992. Imaging spectrocopy for vegetation studies. In: Toselli, F., Bodechtel, J. (Eds.), Imaging Spectrocopy: Fundamentals and Prospective Applications. EAEC, Brussels and Luxembourg. The Netherlands, pp. 145–165.

Hale, G.M., Querry, M.R., 1973. Optical constants of water in the 200 nm to 200 μm wavelength region. Applied Optics 12, 555–563.

Han, L., Rundquist, D.C., 2003. The spectral responses of *Ceratophyllum demersum* at varying depths in an experimental tank. International Journal of Remote Sensing 24, 859–864, Hetch, E., 2000. Óptica. Pearson (Ed.). 720 pp.

Jacquemoud, S., Baret, F., 1990. PROSPECT: a model of leaf optical properties spectra. Remote Sensing of Environment 34, 75–91.

Jacquemoud, S., Bacour, C., Poilve, H., Frangi, J.-P., 2000. Comparison of four radiative transfer models to simulate plant canopies reflectance: direct and inverse mode. Remote Sensing of Environment 74, 471–481.

Jacquemoud, S., Ustin, S.L., Verdebout, J., Schmuck, G., Andreoli, G., Hosgood, B., 1996. Estimating leaf biochemistry using the PROSPECT leaf optical properties model. Remote Sensing of Environment 56, 194–202.

Jacquemoud, S., Verhoef, W., Baret, F., Bacour, C., Zarco-Tejada, P., Asner, G.P., François, C., Ustin, S.L., 2009. PROSPECT + SAIL models: a review of use for vegetation characterization. Remote Sensing of Environment 113, S56–S66.

Jerlov, N.G., 1968. Optical Oceanography. American Elsevier Publ. Co. Inc., New York, 194 pp.

Kallel, A., Le Hégarat-Mascle, S., Ottlé, C., Hubert-Moy, L., 2007. Determination of vegetation cover fraction by inversion of a four-parameter model based on isoline parametrization. Remote Sensing of Environment 111, 553–566.

Kopelevich, O.V., 1976. Optical properties of pure water in the 250–600 nm range. Optical Spectroscopy 41, 391–392.

Kou, L., Labrie, D., Chylek, P., 1993. Refractive indices of water and ice in the 0.65–2.5 μm spectral range. Applied Optics 32, 3531–3540.

Kuusk, A., 1985. The hot spot effect of a uniform vegetative cover. Sovietic Journal of Remote Sensing 3, 645–658.

Landau, L.D., Lifshitz, E.M., 1984. Electrodynamics of Continuous Media, 2nd edition. Pergamon Press, Oxford, England, 460 pp.

Moreau, S., Le Toan, T., 2003. Biomass quantification of Andean wetland forages using ERS satellite SAR data for optimizing livestock management. Remote Sensing of Environment 84, 477–492.

Morel, A., Prieur, L., 1977. Analysis of variations in ocean color. Limnology and Oceanography 22, 709–722.

Oguro, Y., Suga, Y., Takeuchi, S., Ogawa, H., Tsuchiya, K., 2003. Monitoring of a rice field using Landsat-5 TM and Landsat-7 ETM+ data. Advanced Space Research 32, 2223–2228.

Palmer, K.F., Williams, D., 1974. Optical properties of water in the near infrared. Optical Society of America Journal 64, 1107–1110.

Pinty, B., Widlowski, J.-L., Taberner, M., Gobron, N., Verstraete, M.M., Disney, M., Gascon, F., Gastellu, J.-P., Jiang, L., Kuusk, A., Lewis, P., Li, X., Ni-Meister, W., Nilson, T., North, P., Qin, W., Su, L., Tang, S., Thompson, R., Verhoef, W., Wang, H., Wang, J., Yan, G., Zang, H., 2004. RAdiation transfer Model Intercomparison (RAMI) exercise: results from the second phase. Journal of Geophysical Research 109, D06210, http://dx.doi.org/10.1029/2003JD004252.

Pinty, B., Gobron, N., Widlowski, J.-L., Gerstl, S.A.W., Verstraete, M.M., Antunes, M., Bacour, C., Gascon, F., Gastellu, J.-P., Goel, N., Jacquemoud, S., North, P., Qin, W., Thompson, R., 2001. Radiation transfer model intercomparison (RAMI) exercise. Journal of Geophysical Research 106, 11,937–11,956, http://dx.doi.org/10.1029/2000JD900493, D11.

Pope, R.M., Fry, E.S., 1997. Absorption spectrum (380–700 nm) of pure water. II. Integrating cavity measurements. Applied Optics 36, 8710–8723.

Schaepman-Strub, G., Schaepman, M.E., Painter, T.H., Dangel, S., Martonchik, J.V., 2006. Reflectance quantities in optical remote sensing—definitions and case studies. Remote Sensing of Environment 103, 27–42.
Segelstein, D.J., 1981. The Complex Refractive Index of Water. University of Missouri-Kansas City.
Sims, D.A., Gamon, J.A., 2003. Estimation of vegetation water content and photosynthetic tissue area from spectral reflectance: a comparison of indices based on liquid water and chlorophyll absorption features. Remote Sensing of Environment 84, 526–537.
Smith, R.C., Baker, K.S., 1981. Optical properties of the clearest natural waters (200–800 nm). Applied Optics 20, 177–184.
Sogandares, F.M., Fry, E.S., 1997. Absorption spectrum (340–640 nm) of pure water. Photothermal. I. Measurements. Applied Optics 36, 8699–8709.
Sullivan, S.A., 1963. Experimental study of the absorption in distilled water, artificial sea water, and heavy water in the visible region of the spectrum. Optical Society of America Journal 53, 962–968.
van de Hulst, H.C., 1981. Light Scattering by Small Particles. Dover Publications Inc., New York.
Verhoef, W., 1984. Light scattering by leaf layers with application to canopy reflectance modeling: the SAIL model. Remote Sensing of Environment 16, 125–141.
Verhoef, W., 1985. Earth observation modeling based on layer scattering matrices. Remote Sensing of Environment 17, 165–178.
Weiss, M., Baret, F., Myneni, R.B., Pragnère, A., Knyazikhin, Y., 2000. Investigation of a model inversion technique to estimate canopy biophysical variables from spectral and directional reflectance data. Agronomie 20, 3–22.
Widlowski, J.-L., Taberner, M., Pinty, B., Bruniquel-Pinel, V., Disney, M., Fernandes, R., Gastellu-Etchegorry, J.-P., Gobron, N., Kuusk, A., Lavergne, T., Leblanc, S., Lewis, P., Martin, E., Mottus, M., North, P.J.R., Qin, W., Robustelli, M., Rochdi, N., Ruiloba, R., Soler, C., Thompson, R., Verhoef, W., Verstraete, M.M., Xie, D., 2007. The third RAdiation transfer Model Intercomparison (RAMI) exercise: documenting progress in canopy reflectance modelling. Journal of Geophysical Research 112, D0911, http://dx.doi.org/10.1029/2006JD007821.
Wieliczka, D.M., Weng, S., Querry, M.R., 1989. Wedge shaped cell for highly absorbent liquids: infrared optical constants of water. Applied Optics 28, 1714–1719 .
Xiao, X., Boles, S., Liu, J., Zhuang, D., Frolking, S., Li, C., Salas, W., Moore III, B., 2005. Mapping paddy rice agriculture in southern China using multi-temporal *MODIS* images. Remote Sensing of Environment 95, 480–492.
Yebra Álvarez, M., 2008. Estimación del contenido de humedad de vegetación mediterránea a partir de imágenes MODIS. Tesis doctoral Programa de doctorado de Cartografía, S.I.G. y Teledetección de la Universidad de Alcalá de Henares, 191 pp.